

CONTINUUM QCD AND LIGHT MESONS

P. MARIS

Dept. of Physics, Kent State University, Kent, OH 44242
E-mail: maris@faisun.kent.edu

The ladder-rainbow truncation of the set of Dyson–Schwinger equations is used to study light mesons. The parameters in the effective interaction are constrained by the chiral condensate and f_π ; the current quark masses are fitted to m_π and m_K . The dressed quark propagators are in qualitative agreement with recent lattice-QCD results at low q^2 while having the correct perturbative behavior at large q^2 . The resulting vector meson masses are within 5% of the experimental values. The obtained electromagnetic form factors and strong and electroweak coupling constants are also in good agreement with the data. At finite temperature, this truncation leads to a mean-field chiral phase transition. The spatial pion mass is almost constant below this transition, but rises with T close to and above T_c . The mass of its chiral partner, an idealized σ meson, decreases with T until T_c , where it becomes degenerate with the pion.

1 Introduction

Our aim is to obtain the hadron mass spectrum and observables such as coupling constants and form factors from the underlying theory, QCD. The set of Dyson–Schwinger equations [DSEs] form a useful tool for this purpose^{1,2}. In rainbow-ladder truncation, they have been successfully applied to calculate the masses and decay constants of light pseudoscalar and vector mesons^{3,4}. The dressed-quark propagator, as obtained from its DSE, together with the Bethe–Salpeter amplitude [BSA] and the $q\bar{q}\gamma$ vertex as obtained from the homogeneous and inhomogeneous Bethe–Salpeter equations [BSE] respectively, form the necessary elements for form factor calculations in impulse approximation^{5,6}. Extensions to other mesons, and calculations of strong and electroweak decays and branching ratios are straightforward^{7,8}.

At finite temperature chiral symmetry is expected to be restored, and quarks (and gluons) become deconfined. Since the properties of the pion are closely tied to the dynamical breaking of chiral symmetry, an elucidation of the T -dependence of these properties is important; particularly since a prodigious number of pions is produced in heavy ion collisions. Encouraged by the success of the DSE approach to zero-temperature pion physics, see in Sec. 2, we have extended this approach to nonzero temperature⁹, and this is discussed in Sec. 3.

The DSE for the renormalized quark propagator in Euclidean space is

$$S(p)^{-1} = i Z_2 \not{p} + Z_4 m(\mu) + Z_1 \int^{\Lambda} \frac{d^4 q}{(2\pi)^4} g^2 D_{\mu\nu}(k) \frac{\lambda^a}{2} \gamma_\mu S(q) \Gamma_\nu^a(q, p), \quad (1)$$

where $D_{\mu\nu}(k)$ is the dressed-gluon propagator, $\Gamma_\nu^a(q; p)$ the dressed-quark-gluon vertex, and $k = p - q$. The most general solution of Eq. (1) has the form $S(p)^{-1} = i\cancel{p}A(p^2) + B(p^2)$ and is renormalized at spacelike μ^2 according to $A(\mu^2) = 1$ and $B(\mu^2) = m(\mu)$ with $m(\mu)$ the current quark mass. The notation \int^Λ represents a translationally invariant regularization of the integral with Λ the regularization mass-scale; at the end of all calculations this regularization scale can be removed.

Mesons are described by solutions of the homogeneous BSE

$$\Gamma_H(p_+, p_-) = \int^\Lambda \frac{d^4 q}{(2\pi)^4} K(p, q; Q) S(q_+) \Gamma_H(q_+, q_-) S(q_-), \quad (2)$$

where $p_+ = p + \eta Q$ and $p_- = p - (1 - \eta)Q$ are the outgoing and incoming quark momenta respectively, and similarly for q_\pm . The kernel K is the renormalized, amputated $q\bar{q}$ scattering kernel that is irreducible with respect to a pair of $q\bar{q}$ lines. This equation has solutions at discrete values of $Q^2 = -m_H^2$, where m_H is the meson mass. Together with the canonical normalization condition for $q\bar{q}$ bound states, it completely determines Γ_H , the bound state BSA. The different types of mesons, such as (pseudo-)scalar, (axial-)vector, and tensor mesons, are characterized by different Dirac structures. The most general decomposition for pseudoscalar bound states is³

$$\begin{aligned} \Gamma_{PS}(k_+, k_-; P) = \gamma_5 & [iE(k^2; k \cdot P; \eta) + \not{p} F(k^2; k \cdot P; \eta) \\ & + \not{k} G(k^2; k \cdot P; \eta) + \sigma_{\mu\nu} k_\mu P_\nu H(k^2; k \cdot P; \eta)], \end{aligned} \quad (3)$$

where the invariant amplitudes E , F , G and H are Lorentz scalar functions of k^2 and $k \cdot P$. Note that these functions depend on the momentum partitioning parameter η ; however, physical observables are independent of this parameter.

The bound state BSA, together with the dressed quark propagators, are the necessary elements to calculate the electroweak decay constants^{3,4} and, in impulse approximation, strong decays. For describing other electroweak processes one also needs the dressed $q\bar{q}\gamma$ and $q\bar{q}W$ vertices. These vertices satisfy an inhomogeneous BSE: e.g. the $q\bar{q}\gamma$ vertex $\Gamma_\mu(p_+, p_-)$ satisfies

$$\Gamma_\mu(p_+, p_-) = Z_2 \gamma_\mu + \int^\Lambda \frac{d^4 q}{(2\pi)^4} K(p, q; Q) S(q_+) \Gamma_\mu(q_+, q_-) S(q_-). \quad (4)$$

Solutions of the homogeneous version of Eq. (4) define vector meson bound states at timelike photon momenta $Q^2 = -m_v^2$. It follows that $\Gamma_\mu(p_+, p_-)$ has poles at those locations.

2 Model Calculations

To solve the BSE, we use a ladder truncation, with an effective quark-antiquark interaction that reduces to the perturbative running coupling at large momenta^{3,4}. In conjunction with the rainbow truncation for the quark DSE, the ladder truncation preserves both the vector Ward–Takahashi identity [WTI] for the $q\bar{q}\gamma$ vertex and the axial-vector WTI. The latter ensures the existence of massless pseudoscalar mesons connected with dynamical chiral symmetry breaking³. In combination with impulse approximation, this truncation satisfies electromagnetic current conservation⁶.

2.1 Effective interaction

The ladder truncation of the BSE, Eq. (2), is

$$K(p, q; P) \rightarrow -\mathcal{G}(k^2) D_{\mu\nu}^{\text{free}}(k) \frac{\lambda^i}{2} \gamma_\mu \otimes \frac{\lambda^i}{2} \gamma_\nu, \quad (5)$$

where $D_{\mu\nu}^{\text{free}}(k = p - q)$ is the free gluon propagator in Landau gauge. The corresponding rainbow truncation of the quark DSE, Eq. (1), is given by $\Gamma_\nu^i(q, p) \rightarrow \gamma_\nu \lambda^i/2$ together with $g^2 D_{\mu\nu}(k) \rightarrow \mathcal{G}(k^2) D_{\mu\nu}^{\text{free}}(k)$. This truncation was found to be particularly suitable for the flavor octet pseudoscalar and vector mesons since the next-order contributions in a quark-gluon skeleton graph expansion, have a significant amount of cancellation between repulsive and attractive corrections¹⁰.

The model is completely specified once a form is chosen for the “effective coupling” $\mathcal{G}(k^2)$. We employ the Ansatz⁴

$$\frac{\mathcal{G}(k^2)}{k^2} = \frac{4\pi^2 D k^2}{\omega^6} e^{-k^2/\omega^2} + \frac{4\pi^2 \gamma_m \mathcal{F}(k^2)}{\frac{1}{2} \ln \left[\tau + (1 + k^2/\Lambda_{\text{QCD}}^2)^2 \right]}, \quad (6)$$

with $\gamma_m = 12/(33 - 2N_f)$ and $\mathcal{F}(s) = (1 - \exp \frac{-s}{4m_t^2})/s$. The ultraviolet behavior is chosen to be that of the QCD running coupling $\alpha(k^2)$; the ladder-rainbow truncation then generates the correct perturbative QCD structure of the DSE-BSE system of equations. The first term implements the strong infrared enhancement in the region $0 < k^2 < 1 \text{ GeV}^2$ phenomenologically required¹¹ to produce a realistic value¹² for the chiral condensate of about $(240 \text{ GeV})^3$. We use $m_t = 0.5 \text{ GeV}$, $\tau = e^2 - 1$, $N_f = 4$, $\Lambda_{\text{QCD}} = 0.234 \text{ GeV}$, and a renormalization scale $\mu = 19 \text{ GeV}$ which is well into the perturbative domain^{3,4}. The remaining parameters, $\omega = 0.4 \text{ GeV}$ and $D = 0.93 \text{ GeV}^2$ along with the quark masses, are fitted to give a good description of the chiral condensate, $m_{\pi/K}$ and f_π , see Table 1. Note that all invariant amplitudes of the BSA, see Eq. (3),

Table 1: Results for the light pseudoscalar mesons in GeV.

meson	expt. data		our calculation			γ_5 amplitude E only		
	m_H	f_H	m_H	f_H	\mathcal{R}_H	m_H	f_H	\mathcal{R}_H
chiral	0.0	—	0.0	0.090	1.00	0.0	0.067	1.52
pion	0.139	0.0924	0.138	0.092	0.99	0.121	0.069	1.51
kaon	0.497	0.112	0.496	0.109	0.99	0.436	0.081	1.43
$s\bar{s}$	—	—	0.696	0.129	0.99	0.589	0.099	1.44

are needed to satisfy the axial-vector WTI³: \mathcal{R}_H is the ratio of the residues at the meson pole in the pseudovector and pseudoscalar vertices which appear in this WTI, and should be equal to one. From Table 1 it is also clear that the pseudovector amplitudes F and G do contribute to observables; furthermore, they dominate the asymptotic behavior of the pion electromagnetic form factor¹³.

2.2 Quark propagator

Within this model, the quark propagator reduces to the perturbative propagator in the ultraviolet region. The mass function $M(p^2) = B(p^2)/A(p^2)$ behaves for large p^2 like

$$M(p^2) \simeq \frac{\hat{m}_q}{\left(\frac{1}{2} \ln \left[\frac{p^2}{\Lambda_{\text{QCD}}^2}\right]\right)^{\gamma_m}}, \quad (7)$$

where \hat{m}_q is the renormalization-point-independent explicit chiral-symmetry-breaking mass. In the chiral limit the behavior is qualitatively different

$$M(p^2) \simeq \frac{2\pi^2\gamma_m}{3} \frac{-\langle\bar{q}q\rangle^0}{p^2 \left(\frac{1}{2} \ln \left[\frac{p^2}{\Lambda_{\text{QCD}}^2}\right]\right)^{1-\gamma_m}}, \quad (8)$$

with $\langle\bar{q}q\rangle^0$ the renormalization-point-independent chiral condensate³. At one-loop, it is related to the renormalization-dependent condensate

$$\langle\bar{q}q\rangle^\mu = -Z_4 N_c \int^\Lambda \frac{d^4 p}{(2\pi)^4} \text{Tr}[S_{\text{chiral}}(p)], \quad (9)$$

via $\langle\bar{q}q\rangle^\mu = (\ln \mu/\Lambda_{\text{QCD}})^{\gamma_m} \langle\bar{q}q\rangle^0$.

In the infrared region both $Z(p^2) = 1/A(p^2)$ and $M(p^2)$ deviate significantly from the perturbative behavior, due to chiral symmetry breaking. Qualitatively, our results are similar to those obtained in recent lattice simulations¹⁴,

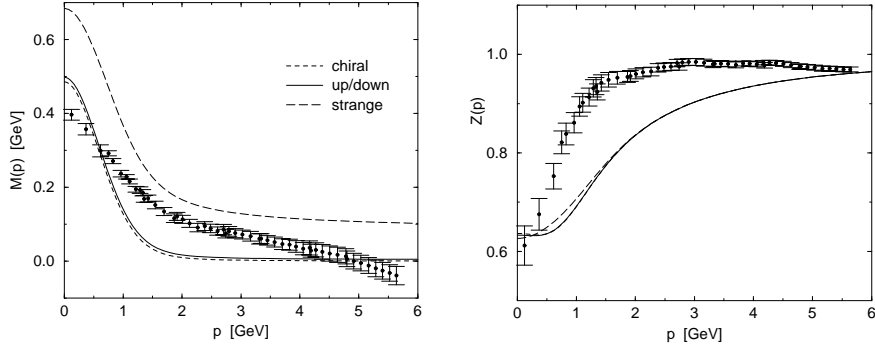


Figure 1: The quark functions $M(p)$ (left) and $Z(p)$ (right), compared to lattice data¹⁴. The lattice data correspond to a bare quark mass of 112 MeV, which is between our up/down and strange quark mass. Note that the lattice data for $M(p)$ are unreliable above $p \approx 1.5$ GeV.

see Fig. 1. The strong enhancement of $M(p^2)$ in the infrared region is a characteristic signal for dynamical chiral symmetry breaking. Also the behavior of $Z(p^2)$ is characteristic: at large p^2 , $Z(p^2) = 1$ up to logarithmic corrections, whereas DSE studies typically find $Z(0)$ to be significantly smaller than one¹⁵. This strongly decreased value of $Z(0)$ is now confirmed by lattice data. The main difference between our results and the lattice data is the onset of the deviation from the perturbative behavior, both for $M(p)$ and for $Z(p)$; this mass scale does depend on details of the effective interaction $\mathcal{G}(k^2)$.

2.3 Meson Masses and Decay Constants

Within the same model, we can now solve the BSE for vector mesons, and calculate the vector meson masses and decay constants. The ρ and ϕ electroweak decay constants are related to the $\rho - \gamma$ and $\phi - \gamma$ coupling constants respectively; the decay constant for the K^* can be extracted from τ -decay into a neutrino and a K^* via a W -boson. The results of our model calculations⁴ are shown in Table 2, and are in reasonable agreement with the data. Corrections

Table 2: Overview of results for light vector meson masses and decay constants, all in GeV.

	m_ρ	f_ρ	m_{K^*}	f_{K^*}	m_ϕ	f_ϕ
expt. data ¹⁶	0.770	0.216	0.892	0.225	1.020	0.236
calculation	0.742	0.207	0.936	0.241	1.072	0.259

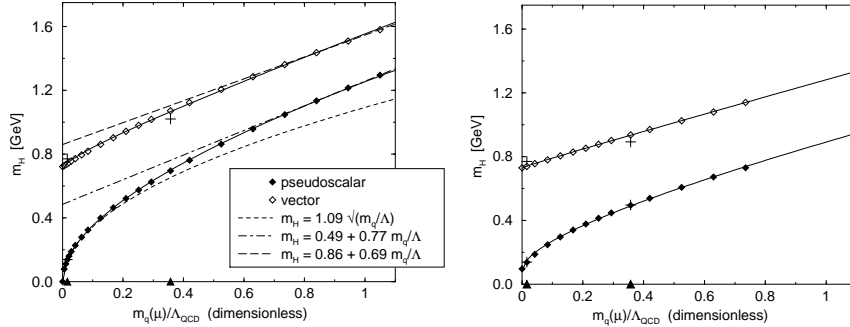


Figure 2: Pseudoscalar and vector meson masses as function of m_q/Λ_{QCD} : left, mesons with equal-mass constituents; right, mesons consisting of one u/d quark and one quark with variable mass m_q . The current quark mass $m_q(\mu)$ are evaluated at $\mu = 19$ GeV; realistic u/d and s quark masses are indicated by triangles, and the corresponding mesons by plusses.

from pseudoscalar meson loops are estimated to be small¹⁷, and will generate a nonzero width for the vector mesons.

Although nature provides us with data for fixed quark masses only, it is interesting to see how observables such as meson masses vary with current quark mass, in particular for comparison with other nonperturbative methods such as lattice QCD. As can be seen from Fig. 2, the pseudoscalar meson mass m_{PS} behaves like $(m_{PS})^2 \propto m_q$ in the limit $m_q \rightarrow 0$, as expected from the Gell-Mann–Oakes–Renner [GMOR] relation. Around the strange quark mass, the curve starts to deviate significantly from this GMOR behavior, and a more linear dependence of the meson mass on m_q begins to emerge¹⁸. This is in agreement with general expectations that for large m_q , meson masses are simply proportional to the current quark mass. The vector meson masses show a much more linear dependence on m_q . Over the current mass range explored, our results for both the vector and the pseudoscalar mesons can be fitted by a form $m_H = \alpha + \beta \sqrt{m_q/\Lambda_{\text{QCD}}} + \gamma m_q/\Lambda_{\text{QCD}}$, with the parameters of Table 3.

Table 3: Fitted parameters for the mesons mass dependence on m_q (in GeV).

	m_π	m_ρ	m_K	m_{K^*}
α	0.0	0.703	0.083	0.728
β	1.04	0.25	0.50	0.03
γ	0.21	0.61	0.31	0.52

The decay constants all grow with m_q , at least in the range of current quark masses explored. In the heavy quark limit, one can show analytically that the pseudoscalar and vector decay constants vanish like $1/\sqrt{m_q}$, as expected from heavy quark effective theory⁸. The turn-over point for this behavior is larger than three times the strange quark mass, at least in the present model. The details of this turn-over do of course depend on the details of the effective interaction. However, the qualitative behavior, both of the meson masses and of the decay constants, is expected to be model-independent.

2.4 Meson Form Factors

Meson electromagnetic form factors in impulse approximation are described by two diagrams, with the photon coupled to the quark and to the antiquark respectively. We can define a form factor for each of these diagrams⁶, e.g.

$$2 P_\nu F_{a\bar{b}\bar{b}}(Q^2) = N_c \int \frac{d^4 q}{(2\pi)^4} \text{Tr} [S^a(q) \Gamma_{\text{ps}}^{a\bar{b}}(q, q_+; P_-) \\ \times S^b(q_+) i\Gamma_\nu^b(q_+, q_-) S^b(q_-) \bar{\Gamma}_{\text{ps}}^{a\bar{b}}(q_-, q; -P_+)] , \quad (10)$$

where $q = k + \frac{1}{2}P$, $q_\pm = k - \frac{1}{2}P \pm \frac{1}{2}Q$, $P_\pm = P \pm \frac{1}{2}Q$. We work in the isospin symmetry limit, so for the pion form factor we have $F_\pi(Q^2) = F_{u\bar{u}u}(Q^2)$. The charged and neutral kaon form factors are given by $F_{K^+} = \frac{2}{3}F_{u\bar{s}u} + \frac{1}{3}F_{u\bar{s}\bar{s}}$ and $F_{K^0} = -\frac{1}{3}F_{d\bar{s}d} + \frac{1}{3}F_{d\bar{s}\bar{s}}$ respectively. Our results for $Q^2 F_\pi$, $Q^2 F_{K^+}$, and $Q^2 F_{K^0}$ are shown in Fig. 3, with the charge radii are given in Table 4.

Up to about $Q^2 = 3 \text{ GeV}^2$, our results for F_π and F_K can be fitted quite well by a monopole. Asymptotically, these functions behave like $Q^2 F(Q^2) \rightarrow c$ up to logarithmic corrections. However, numerical limitations prevent us from accurately determining these constants. Around $Q^2 = 3 \text{ GeV}^2$, our result for $Q^2 F_\pi$ is well above the pQCD result²³ $16\pi f_\pi^2 \alpha_s(Q^2) \sim 0.2 \text{ GeV}^2$, and clearly not yet asymptotic. If we continue the calculation for the electromagnetic form factor into the timelike region, we find a pole at the mass of the vector meson bound states. Using the behavior of $F_{u\bar{u}u}$ and $F_{u\bar{s}\bar{s}}$ around this pole, we can

Table 4: Overview of calculated meson charge radii in fm^2 , with expt. data²², and meson coupling constants, with expt. values extracted from decay widths¹⁶.

	r_π^2	$r_{K^+}^2$	$r_{K^0}^2$	$r_{\pi\gamma\gamma}^2$	$g_{\pi\gamma\gamma}$	$g_{\rho\pi\gamma}$	$g_{\rho\pi\pi}$	$g_{\phi KK}$
expt. data	0.44	0.34	-0.054	0.42	0.50	0.57	6.02	4.64
calculation	0.45	0.38	-0.086	0.39	0.50	0.54	4.85	4.63

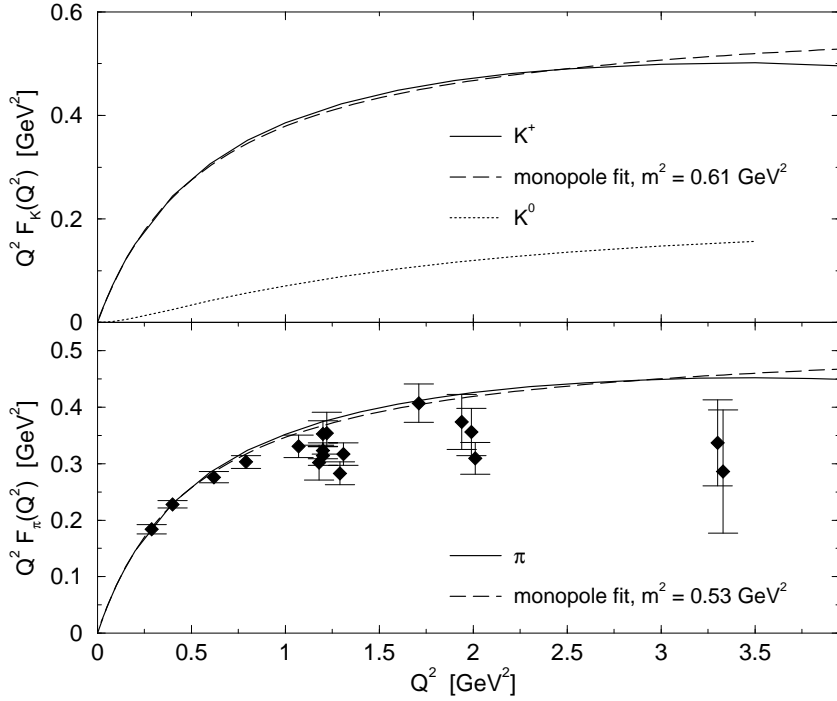


Figure 3: The electromagnetic form factors of the light pseudoscalar mesons⁶. The pion data shown here are from an analysis by Bebek *et al.*¹⁹. Our results are in good agreement with preliminary new data from JLab for the pion²⁰; new results for F_{K+} are also expected²¹.

extract the coupling constants $g_{\rho\pi\pi}$ and $g_{\phi KK}$ respectively²⁴, which govern the strong decays $\rho \rightarrow \pi\pi$ and $\phi \rightarrow KK$. The results from this analysis are also given in Table 4, and are reasonably close to the experimental data.

The impulse approximation for the $\gamma^*\pi\gamma$ vertex with γ^* momentum Q is

$$\begin{aligned} \Lambda_{\mu\nu}(P, Q) &= i \frac{\alpha}{\pi f_\pi} \epsilon_{\mu\nu\alpha\beta} P_\alpha Q_\beta g_{\pi\gamma\gamma} F_{\gamma^*\pi\gamma}(Q^2) \\ &= \frac{N_c}{3} \int \frac{d^4 q}{(2\pi)^4} \text{Tr} [S(q) i\Gamma_\nu(q, q') S(q') i\Gamma_\mu(q', q'') S(q'') \Gamma_\pi(q'', q; P)] . \end{aligned} \quad (11)$$

where the momenta follow from momentum conservation. In the chiral limit, the value at $Q^2 = 0$, corresponding to the decay $\pi^0 \rightarrow \gamma\gamma$, is given by the axial anomaly and its value $g_{\pi\gamma\gamma}^0 = \frac{1}{2}$ is a direct consequence of only gauge invariance and chiral symmetry; this value is reproduced by our calculations¹³ and

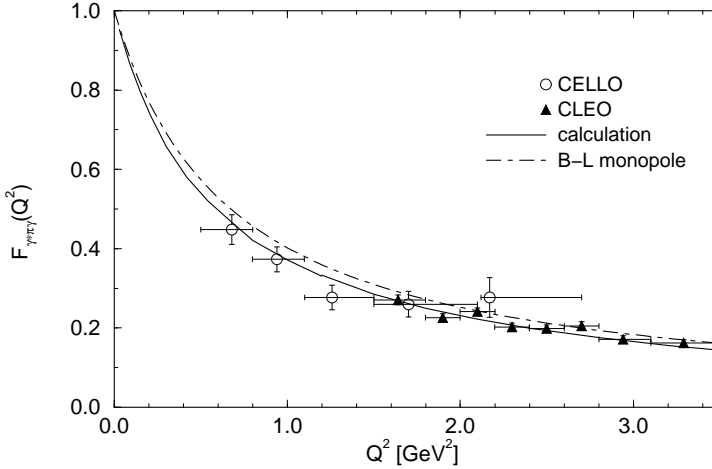


Figure 4: The $\gamma^* \pi\gamma$ form factor²⁵, with data from CLEO and CELLO²⁶.

corresponds well with the experimental width of 7.7 eV. In Fig. 4 we show our results with realistic quark masses, normalized to the experimental $g_{\pi\gamma\gamma}$. The large- Q^2 behavior of $F_{\gamma^* \pi\gamma}$ lies in between monopoles fitted to the Brodsky–Lepage pQCD asymptotic limit²⁷, $8\pi^2 f_\pi^2$, and the limit obtained from a naive analysis of the impulse approximation within the DSE approach^{28,29}, $\frac{16}{3}\pi^2 f_\pi^2$. Our results for $F_{\gamma^* \pi\gamma}$ are compatible with an estimate for the asymptotic behavior by Anikin *et al.*³⁰.

3 Finite Temperature Extension

In the Matsubara formalism, the quark propagator can be written as

$$S^{-1}(\vec{p}, \omega_k) = i\vec{\gamma} \cdot \vec{p} A(p^2, \omega_k^2) + i\gamma_4 \omega_k C(p^2, \omega_k^2) + B(p^2, \omega_k^2) \quad (12)$$

$$= Z_2^A i\vec{\gamma} \cdot \vec{p} + Z_2^C i\gamma_4 \omega_k + Z_4 m(\mu) + \Sigma(\vec{p}, \omega_k), \quad (13)$$

where $\omega_k = (2k + 1)\pi T$ is the fermion Matsubara frequency and T the temperature. The functions A and C are renormalized such that $A(p^2, \omega_0^2) = 1 = C(p^2, \omega_0^2)$, and $B(p^2, \omega_0^2) = m(\mu)$ at $p^2 + \omega_0^2 = \mu^2$. The approximations we use are similar to the $T = 0$ studies discussed in the previous sections. The rainbow-ladder truncation for the self-energy is

$$\Sigma(\vec{p}, \omega_k) = \frac{4}{3}T \sum_{l=-\infty}^{\infty} \int^{\Lambda} \frac{d^3 q}{(2\pi)^3} g^2 D_{\mu\nu}(\vec{p} - \vec{q}, \Omega_{k-l}) \gamma_\mu S(\vec{q}, \omega_l) \gamma_\nu, \quad (14)$$

where $g^2 D_{\mu\nu}$, the effective interaction or effective gluon propagator, at finite T is taken to be the minimal extension of a $T = 0$ model^{9,31,32} with all parameters fixed at $T = 0$. This truncation leads to a second-order chiral phase transition

$$\langle \bar{q}q \rangle^0 \propto (1 - T/T_c)^\beta, \quad T/T_c \uparrow 1, \quad (15)$$

where β is the critical exponent for chiral symmetry restoration. Independent of the details of the effective interaction, we find mean field behavior, $\beta = 1/2$, in rainbow-ladder models³². However, one has to go to extremely small current quark masses, several orders of magnitude smaller than realistic u/d quark masses, to observe this mean-field behavior. The critical temperature is sensitive to details of the model, but with the model parameters fitted to $T = 0$ pion observables, one typically finds $T_c \sim 0.15$ GeV.

3.1 Meson correlations at finite temperature

In order to study meson correlations⁹ we solve the inhomogeneous scalar and pseudoscalar vertices $\Gamma_{S,PS}$ for the lowest external (meson) Matsubara mode, $\Omega_0 = 0$. Bound states will appear as poles in these vertices; for this choice of the external momentum these poles correspond to the spatial modes, and thus the masses to the spatial masses^{9,33}, which are the type of masses that are usually calculated in lattice simulations.

For $\hat{m} = 0$ the $T = 0$ inhomogeneous BSEs exhibit poles at $m_\pi = 0$ and $m_\sigma = 0.56$ GeV, with $m_\sigma = 0.59$ GeV at $\hat{m} = 5.7$ MeV. This low-mass scalar is typical of the rainbow-ladder truncation, although there is some model sensitivity. The rainbow-ladder truncation yields degenerate isoscalar and isovector bound states, and ideal flavor mixing in the 3-flavor case; improvements beyond the ladder truncation are required in order to describe the observed scalar mesons. Furthermore, in the isoscalar-scalar channel, it will be necessary to include couplings to the dominant $\pi\pi$ mode³⁴ because of the large σ width. In the absence of such corrections, the σ properties elucidated herein are strictly only those of an idealized chiral partner of the π .

These poles evolve with T in such a way⁹ that at the critical temperature, we have degenerate, massless pseudoscalar and scalar bound states, see Fig. 5. Above T_c , these bound states persist, becoming increasingly massive with increasing T and approaching $2\pi T$, the thermal mass of two free quarks. Similar features are also observed in numerical simulations of lattice-QCD³⁵. Above T_c all but the leading Dirac amplitude vanishes and the surviving pseudoscalar amplitude is pointwise identical to the surviving scalar one. These results indicate that the chiral partners are *locally* identical above T_c , they do not just have the same mass. Approaching T_c from below, our analysis yields for the

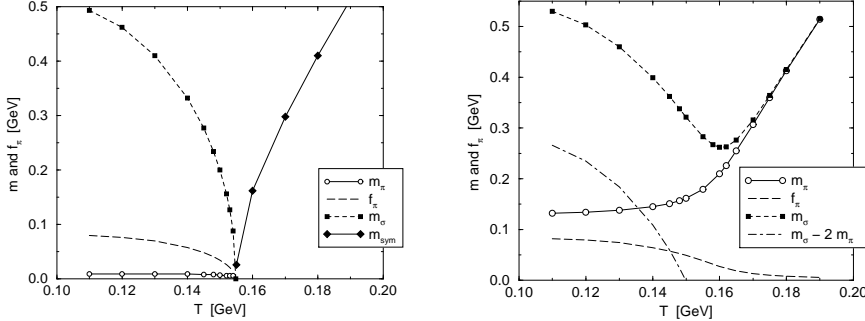


Figure 5: The π and σ mass, decay constant as function of T , both in the chiral limit (left) and with realistic current quark mass (right)⁹.

σ mass $m_\sigma \propto (1 - T/T_c)^\beta$ within numerical errors. Note that this is the same behavior as the chiral condensate and other, equivalent order parameters for chiral symmetry restoration, such as the decay constant f_π .

For nonzero current-quark masses chiral symmetry restoration is exhibited as a crossover rather than a phase transition. That the transition has become a crossover is evident in the behavior of f_π , see the right panel of Fig. 5. The σ mass exhibits a dip around the phase transition. The scalar and pseudoscalar meson masses become indistinguishable at $T \sim 1.2 T_c$.

With the BSAs obtained from the homogeneous BSE, we can now calculate the T -dependence of other meson properties⁹. The T -dependence of $g_{\pi\gamma\gamma}$ is calculated in a similar fashion as at $T = 0$ in the previous section. At $T = 0$ this coupling saturates the Abelian anomaly: $g_{\pi\gamma\gamma} = \frac{1}{2}$. The interesting quantity is: $g_{\pi\gamma\gamma}^0/f_\pi^0$, which vanishes at T_c in the chiral limit³⁶: $g_{\pi\gamma\gamma}^0$ goes to zero linearly. Thus, in the chiral limit, the coupling to the dominant decay channel closes for both charged and neutral pions. For $\hat{m} \neq 0$ both the coupling: $g_{\pi\gamma\gamma}/f_\pi$, and the corresponding width exhibit a crossover with a slight enhancement in the width as $T \rightarrow T_c$ due to the increase in m_π .

Also the isoscalar-scalar- $\pi\pi$ strong coupling vanishes at T_c in the chiral limit, which can be traced to $B_{\text{chiral}} \rightarrow 0$. For $\hat{m} \neq 0$, the coupling reflects the crossover. However, that is irrelevant because the width vanishes just below T_c where the σ meson mass falls below $2m_\pi$ and the phase space factor vanishes. A similar phenomenon occurs for the $\rho\pi\pi$ decay width: with a separable model for the effective interaction it was shown³³ that slightly above T_c the spatial mass of the ρ becomes smaller than $2m_\pi$, and thus the strong decay of a ρ into pions becomes impossible because of phase space consideration. However, one

should keep in mind that these are the spatial masses, and that effects such as collisional broadening are not yet taken into account.

Acknowledgments

I would like to thank Wolfgang Lucha and Kim Maung Maung for their efforts in organizing this conference. I am also grateful to the Erwin Schroedinger Institute for Mathematical Physics in Vienna for their hospitality and financial support. Most of the work discussed here was done in collaboration with Peter Tandy and Craig Roberts; I would also like to thank Tony Williams, Sebastian Schmidt, Dennis Jarecke, and David Blaschke for useful discussions. This work was funded by the National Science Foundation under grants Nos. INT-9603385 and PHY97-22429, and benefited from the resources of the National Energy Research Scientific Computing Center.

References

1. C. D. Roberts and S. M. Schmidt, nucl-th/0005064.
2. R. Alkofer and L. von Smekal, hep-ph/0007355.
3. P. Maris and C. D. Roberts, Phys. Rev. **C56**, 3369 (1997).
4. P. Maris and P. C. Tandy, Phys. Rev. **C60**, 055214 (1999).
5. P. Maris and P. C. Tandy, Phys. Rev. **C61**, 045202 (2000).
6. P. Maris and P. C. Tandy, nucl-th/0005015, Phys. Rev. **C**, in press.
7. C. J. Burden *et al.* Phys. Rev. **C55**, 2649 (1997); Y. Kalinovsky, K. L. Mitchell and C. D. Roberts, Phys. Lett. **B399**, 22 (1997); J. C. Bloch, Y. L. Kalinovsky, C. D. Roberts and S. M. Schmidt, Phys. Rev. **D60**, 111502 (1999).
8. M. A. Ivanov, Y. L. Kalinovsky and C. D. Roberts, Phys. Rev. **D60**, 034018 (1999).
9. P. Maris, C. D. Roberts, S. M. Schmidt and P. C. Tandy, nucl-th/0001064.
10. A. Bender, C. D. Roberts and L. von Smekal, Phys. Lett. **B380**, 7 (1996).
11. F. T. Hawes, P. Maris and C. D. Roberts, Phys. Lett. **B440**, 353 (1998).
12. D. B. Leinweber, Annals Phys. **254**, 328 (1997).
13. P. Maris and C. D. Roberts, Phys. Rev. **C58**, 3659 (1998).
14. J. I. Skullerud and A. G. Williams, hep-lat/0007028; these proceedings.
15. C. D. Roberts, nucl-th/0007054, Contribution to the proceedings of the Confinement Research Program at the Erwin Schroedinger Institute for Mathematical Physics, Vienna, Austria, Coordinated by W. Lucha, A. Martin and F. Schoeberl, May-July, 2000.
16. Particle Data Group, C. Caso *et al.*, Eur. Phys. J. **C3**, 1 (1998).

17. L.C.L. Hollenberg, C.D. Roberts and B.H.J. McKellar, Phys. Rev. **C 46**, 2057 (1992); K.L. Mitchell and P.C. Tandy, Phys. Rev. **C 55**, 1477 (1997); M.A. Pichowsky, S. Walawalkar and S. Capstick, Phys. Rev. **D 60**, 054030 (1999).
18. P. Maris and C. D. Roberts, nucl-th/9710062, in the proceedings of the IVth Int. Workshop on Progress in Heavy Quark Physics, Sept. 1997, Rostock, BRD, edited by M. Beyer, T. Mannel, and H. Schröder (1998).
19. C. J. Bebek *et al.*, Phys. Rev. **D17**, 1693 (1978).
20. J. Volmer, *The pion charge form factor via pion electroproduction on the proton*, PhD thesis, Amsterdam 2000.
21. G. Niculescu *et al.*, Phys. Rev. Lett. **81**, 1805 (1998); O. K. Baker, these proceedings.
22. S. R. Amendolia *et al.* [NA7 Collaboration], Nucl. Phys. **B277**, 168 (1986); S. R. Amendolia *et al.*, Phys. Lett. **B178**, 435 (1986); W. R. Molzon *et al.*, Phys. Rev. Lett. **41**, 1213 (1978).
23. G. R. Farrar and D. R. Jackson, Phys. Rev. Lett. **43**, 246 (1979).
24. P. Maris and P.C. Tandy, KSUCNR-109-00, in progress, Contribution to the proceedings of the Confinement Research Program at the Erwin Schrödinger Institute for Mathematical Physics, Vienna, Austria, Co-ordinated by W. Lucha, A. Martin and F. Schoeberl, May-July, 2000.
25. P. Maris, nucl-th/0008048, to appear in the proceedings of the Xth Light-Cone Meeting on Non-Perturbative QCD and Hadron Phenomenology, Heidelberg, BRD, June 2000.
26. H. J. Behrend *et al.* [CELLO Collaboration], Z. Phys. **C49**, 401 (1991); J. Gronberg *et al.* [CLEO Collaboration], Phys. Rev. **D57**, 33 (1998).
27. G. P. Lepage and S. J. Brodsky, Phys. Rev. **D22**, 2157 (1980).
28. D. Kekez and D. Klabucar, Phys. Lett. **B457**, 359 (1999).
29. C. D. Roberts, Fizika **B8**, 285 (1999); P. C. Tandy, Fizika **B8**, 295 (1999); D. Klabucar and D. Kekez, Fizika **B8**, 303 (1999).
30. I. V. Anikin, A. E. Dorokhov and L. Tomio, Phys. Lett. **B475**, 361 (2000).
31. A. Bender, D. Blaschke, Y. Kalinovsky and C. D. Roberts, Phys. Rev. Lett. **77**, 3724 (1996).
32. A. Holl, P. Maris and C. D. Roberts, Phys. Rev. **C59**, 1751 (1999).
33. D. Blaschke *et al.*, nucl-th/0002024.
34. M. R. Pennington, hep-ph/0001183.
35. E. Laermann, Fiz. Élem. Chastits At. Yadra **30**, 720 (1999) (Phys. Part. Nucl. **30**, 304 (1999)).
36. R.D. Pisarski, Phys. Rev. Lett. **76**, 3084 (1996).